The Mechanism of Dienoyl-CoA Reduction by 2,4-Dienoyl-CoA Reductase Is Stepwise: Observation of a Dienolate Intermediate†

Kerry L. Fillgrove and Vernon E. Anderson*

Department of Biochemistry, Case Western Reserve University, Cleveland, Ohio 44106-4935

Received June 5, 2001; Revised Manuscript Received August 17, 2001

ABSTRACT: The chemical mechanism of the 2,4-dienoyl-CoA reductase (EC 1.3.1.34) from rat liver mitochondria has been investigated. This enzyme catalyzes the NADPH-dependent reduction of 2,4-dienoyl-coenzyme A (CoA) thiolesters to the resulting *trans*-3-enoyl-CoA. Steady-state kinetic parameters for *trans*-2,*trans*-4-hexadienoyl-CoA and 5-phenyl-*trans*-2,*trans*-4-pentadienoyl-CoA were determined and demonstrated that the dienoyl-CoA and NADPH bind to the 2,4-dienoyl-CoA reductase via a sequential kinetic mechanism. Kinetic isotope effect studies and the transient kinetics of substrate binding support a random order of nucleotide and dienoyl-CoA addition. The large normal solvent isotope effects on V/K ($^{D_2O}V/K$) and V (^{D_2O}V) for *trans*-2,*trans*-4-hexadienoyl-CoA reduction indicate that a proton transfer step is rate limiting for this substrate. The stability gained by conjugating the phenyl ring to the diene in PPD-CoA results in the reversal of the rate-determining step, as evidenced by the normal isotope effects on V/K_{CoA} ($^{D}V/K_{CoA}$) and V/K_{NADPH} ($^{D}V/K_{NADPH}$). The reversal of the rate-determining step was supported by transient kinetics where a burst was observed for the reduction of *trans*-2,*trans*-4-hexadienoyl-CoA but not for 5-phenyl-*trans*-2,*trans*-4-pentadienoyl-CoA reduction. The chemical mechanism is stepwise where hydride transfer from NADPH occurs followed by protonation of the observable dienolate intermediate, which has an absorbance maximum at 286 nm. The exchange of the Cα protons of *trans*-3-decenoyl-CoA, catalyzed by the 2,4-dienoyl-CoA reductase, in the presence of $NADP^+$ suggests that formation of the dienolate is catalyzed by the enzyme active site.

Enoyl-thiolester reductases are involved in many physiological processes but are primarily involved in fatty acid elongation pathways (*1*−*5*). These enzymes have been identified as the primary targets for the antimicrobial agents isoniazid and triclosan (*6*−*10*). Enoyl-thiolester reductases catalyze the NAD(P)H[1]-dependent reduction of the α,β double bond of the enoyl-thiolester to the resulting saturated acyl-thiolester. Unlike the reactions catalyzed by these reductases, the 2,4-dienoyl-CoA reductase (24DCR) catalyzes the unusual 1,4 addition of H_2 across a conjugated diene, producing a *trans*-3-enoyl-CoA product (*11*).

The metabolism of unsaturated fatty acids requires several auxiliary enzymes in addition to the enzymes associated with the traditional β-oxidation spiral. The metabolism of most unsaturated fatty acids proceeds through a pathway requiring the 2,4-dienoyl-CoA reductase. Naturally occurring fatty acids possess cis double bonds in contrast to trans double bonds present in partially hydrogenated vegetable oils (*12*, *13*). A correlation between diets containing high levels of trans fatty acids and coronary heart disease has been previously reported (*14*), which makes the characterization of trans fatty acid metabolism of particular interest. The 24DCR is involved in the metabolism of all unsaturated fatty acids with double bonds originating at even-numbered positions (*15*, *16*) and the majority of unsaturated fatty acids with double bonds originating at odd-numbered positions (*17*, *18*), regardless of the stereochemical configuration of the double bonds. Interestingly, this enzyme catalyzes the reduction of *trans*-2-, *cis*-4-, and *trans*-2,*trans*-4-dienoyl-CoAs with nearly equivalent efficacy (*19*−*21*).

The stereochemical course of the reactions catalyzed by enoyl-thiolester reductases has been extensively studied (*11*, *22*−*25*), but until recently there have been few reports characterizing the catalytic mechanism. The InhA enoyl-thiolester reductase from *Mycobacterium tuberculosis* has been intensively studied (*5*, *26*), and preliminary studies on the InhA homologue from *Brassica napus* have also been reported (*27*). Solvent and primary kinetic isotope effects demonstrated that substrates bind to InhA in a random order (with NADH having a slight preference) and that the mechanism is stepwise, proceeding through an enolate intermediate.

In the present study, steady-state and transient kinetic experiments were performed to obtain the kinetic parameters of the 24DCR. Primary kinetic isotope effects on the hydride transfer from NADPH and solvent isotope effects were used to characterize the chemical mechanism of this enzyme. Transient kinetic studies were performed, and a spectrum

† Supported in part by Grant GM 36562 from the National Institutes of Health. K.L.F. was supported by National Institutes of Health Metabolism Training Grant DK 07319.

* To whom correspondence should be addressed. Phone: (216) 368-2599. Fax: (216) 368-3419. E-mail: anderson@biochemistry.cwru.edu.

[1] Abbreviations: 24DCR, 2,4-dienoyl-CoA reductase; HPLC, high-performance liquid chromatography; $NADP^+$, β-nicotinamide adenine dinucleotide phosphate; NADPH, β-nicotinamide adenine dinucleotide phosphate, reduced form; NMR, nuclear magnetic resonance; SDS−PAGE, sodium dodecyl sulfate−polyacrylamide gel electrophoresis; SVD, single value decomposition; DD-CoA, *trans*-2,*trans*-4-decadienoyl-CoA; HD-CoA, *trans*-2,*trans*-4-hexadienoyl-CoA; PPD-CoA, 5-phenyl-*trans*-2,*trans*-4-pentadienoyl-CoA.

10.1021/bi0111606 CCC: $20.00
Published on Web 09/18/2001

of the dienolate intermediate predicted by the isotope effect studies was observed.

EXPERIMENTAL PROCEDURES

Materials. *trans*-2,*trans*-4-Decadien-1-al, *trans*-2,*trans*-4-hexadienoic acid, and D_2O (99.9 atom % D) were from Aldrich. 5-Phenyl-2,4-pentadienoic acid was from Lancaster. Coenzyme A (lithium salt) was from USB. Dibasic potassium phosphate (K_2HPO_4), sodium bicarbonate, and silver oxide (Ag_2O) were from Fisher Scientific. *Cryptococcus uniguttulatus* glucose dehydrogenase, $NADP^+$, and NADPH were from Sigma. [1-^{2}H]Glucose was from Omicron Biochemicals, Inc. All other reagents were of research grade or better and were obtained from commercial sources.

Synthesis and Purification of CoA Substrates. *trans*-2,*trans*-4-Hexadienoyl-CoA (HD-CoA) and 5-phenyl-*trans*-2,*trans*-4-pentadienoyl-CoA (PPD-CoA) were synthesized from the corresponding fatty acids via the mixed anhydride method (*28*). The dienoyl-CoAs were then purified by reversed-phase HPLC using a 10 × 250 mm Econosil C18 column (Alltech). The CoA thiolesters were eluted with a linear methanol gradient and were detected by the ultraviolet absorbance of the adenine, at 260 nm, and dienoyl-thiolester, at 296 and 340 nm for HD-CoA and PPD-CoA, respectively. The synthesis of *trans*-2,*trans*-4-decadienoyl-CoA (DD-CoA) was performed in a similar manner. The commercially available *trans*-2,*trans*-4-decadien-1-al was oxidized to the corresponding acid with Ag_2O (*29*, *30*). The acid was then used to make the corresponding acyl-CoA via the mixed anhydride method and was purified by reversed-phase HPLC. After purification the HD-CoA, PPD-CoA, and DD-CoA were concentrated to ~1 mM, sparged with helium, and stored frozen at −80 °C. The pure HD-CoA has a 296 nm/260 nm absorbance ratio of 0.94 and the DD-CoA has a 300 nm/260 nm absorbance ratio of 1.01. The PPD-CoA has a 340 nm/260 nm absorbance ratio of 2.11, which is in agreement with the value previously reported by Nada et al. (*31*).

The concentrations of the *trans*-2,*trans*-4-dienoyl-CoA thiolesters were determined using an extinction coefficient at 296 nm of 23 000 M^{-1} cm^{-1} (*32*). The concentration of PPD-CoA was determined using an extinction coefficient at 340 nm of 40 400 M^{-1} cm^{-1} (Fillgrove and Anderson, unpublished results).

Enzymatic Synthesis of trans-3-Decenoyl-CoA. *trans*-3-Decenoyl-CoA was prepared enzymatically by the 24DCR-catalyzed reduction of DD-CoA. To begin, 600 μL of a 1.2 mM DD-CoA solution was combined with 600 μL of potassium phosphate buffer (100 mM, 100 μM EDTA, pH 7.5) containing NADPH (100 μM final concentration). The reaction was initiated by the addition of a catalytic amount of 24DCR and was incubated at room temperature for 15 min, followed by the addition of glucose (6 mM) and glucose dehydrogenase. The reaction was allowed to proceed until there was no longer absorbance at 300 nm. The enzymes were removed by vortexing after the addition of 30 μL of $CHCl_3$. The supernatant after centrifugation was purified by reversed-phase HPLC, and the purified *trans*-3-decenoyl-CoA was taken to dryness by vacuum centrifugation and then stored desiccated at −20 °C.

Synthesis and Purification of [4S-^{2}H]NADPH. [4*S*-^{2}H]-NADPH was prepared enzymatically and purified in the following manner. To begin, 5 mg of $NADP^+$ was added to 2.5 mL of potassium phosphate buffer (100 mM, 100 μM EDTA, pH 8.0) containing [1-^{2}H]glucose (~8 mM). The reaction was initiated by the addition of glucose dehydrogenase from *C. uniguttulatus*, which adds a hydrogen to the *pro-4S* position of $NADP^+$ (*33*). The increase in absorbance at 340 nm was used to monitor the reaction. When there was no further change in the A_{340}, the enzyme was removed by vortexing the reaction solution after the addition of 50 μL of $CHCl_3$. The supernatant after centrifugation was then purified by reversed-phase HPLC using a modified method of Klaidman et al. (*34*). The [4*S*-^{2}H]NADPH was purified using a 4.6 × 250 mm Econosil C18 column (Alltech) that had been equilibrated with buffer A (200 mM NH_4HCO_3, pH 7.6) at a flow rate of 1 mL/min. After the sample was loaded, the column was washed for 15 min at 100% buffer A, followed by a 5 min linear gradient to 15% MeOH in buffer A. The column was washed for 10 min at 15% MeOH in buffer A, followed by a second 5 min linear gradient to 30% MeOH in buffer A. Lastly, the column was washed for 10 min with 30% MeOH in buffer A. The fractions with an A_{260}/A_{340} absorbance ratio less than 2.25 were pooled and desalted as follows. Initially, the concentration of the NH_4HCO_3 buffer in the pooled fractions was increased to approximately 300 mM. The [4*S*-^{2}H]NADPH was loaded onto a 1.0 × 3.4 cm C18 column (Prep Sep, Fisher) and eluted with 20% MeOH in ddH_2O. The desalted [4*S*-^{2}H]-NADPH was then pooled, and 2 equiv of sodium bicarbonate was added followed by lyophilization. The lyophilized [4*S*-^{2}H]NADPH was stored at −80 °C.

Enzymes. The recombinant functional 24DCR was over-expressed in *Escherichia coli* and was purified by the previously described protocol (*32*). The purified enzyme exhibited a single band in Coomassie Blue stained SDS−PAGE and was used without any further manipulation.

Steady-State Kinetics. Steady-state kinetic data were collected using a Hewlett-Packard 8452A diode array spectrophotometer. The decrease in absorbance at 340 nm was monitored as a function of time, and an $\epsilon_{340} = 7820$ M^{-1} cm^{-1} was used for the reduction of HD-CoA (*32*). Similarly, an $\epsilon_{340} = 46\,600$ M^{-1} cm^{-1} was used for the reduction of PPD-CoA. These values account for the contributions of both NADPH oxidation and the corresponding dienoyl-CoA reduction to the absorbance at 340 nm.

All assays were conducted in potassium phosphate buffer (100 mM, 100 μM EDTA, pH 7.5) at 25 ± 0.2 °C where the temperature was maintained by a circulating water bath. Initial velocity patterns for HD-CoA reduction were obtained using variable concentrations of NADPH (10−100 μM) and dienoyl-CoA (1−30 μM). Likewise, the initial velocity patterns for PPD-CoA reduction were obtained using variable concentrations of NADPH (1−90 μM) and dienoyl-CoA (0.3−12 μM). For each dienoyl-CoA substrate all data points were simultaneously fit to the equations

$$v = \frac{VAB}{K_{ia}K_b + K_aB + K_bA + AB} \quad (1)$$

$$v = \frac{AB}{(V/K_{ia}K_b)^{-1} + B(V/K_a)^{-1} + A(V/K_b)^{-1} + AB(V)^{-1}} \quad (2)$$

using GraFit v3.01 (Erithacus Software Ltd.), where v and V are the initial and maximum velocities, A and B represent substrate concentrations, K_a and K_b are Michaelis constants for A and B, and K_{ia} is the dissociation constant for A. In eq 2 $V/K_{ia}K_b$, V/K_a, and V/K_b are evaluated as individual parameters which enable the standard errors for these values to be reported directly by commercial nonlinear least squares programs.

Preparation of Phosphate Buffer Salts for Solvent Isotope Effect Studies and Transient Kinetics. A solution containing 100 mM K_2HPO_4 and 100 μM EDTA was prepared, and the buffer was titrated to pH 7.1 using HCl. Aliquots (25 mL) of the buffer were taken to dryness by lyophilization, and the dried salts were dissolved in D_2O and again taken to dryness by lyophilization. This process was repeated twice to ensure that the protons had been exchanged for deuterons in the buffer salts. Immediately prior to use, the H → D exchanged salts were dissolved in 25 mL of D_2O and a pD 7.5 was verified (pH meter reading + 0.4) (*35*).

Solvent Kinetic Isotope Effects. Solvent deuterium isotope effects on V (^{D_2O}V) and V/K ($^{D_2O}V/K$) were determined at pD(H) 7.5 in 100 mM KP_i containing 100 μM EDTA. Initial velocity patterns for HD-CoA reduction and PPD-CoA were obtained in both H_2O and D_2O using the variable concentrations of NADPH (10−100 μM) and dienoyl-CoA (1−30 μM). Similarly, initial velocity patterns for PPD-CoA reduction were obtained in both H_2O and D_2O using variable concentrations of NADPH (1−90 μM) and dienoyl-CoA (0.3−12 μM). The H_2O and D_2O initial velocity data obtained for HD-CoA were combined and globally fit to the following equation using GraFit

$$v = VAB/\{(1 + f_i IE_{V/K})[K_{ia}K_b + K_aB + K_bA] + (1 + f_i IE_V)[AB]\} \quad (3)$$

where f_i is the fraction of isotope (^{2}H) in the reaction (0−1.0), $IE_{V/K}$ and IE_V are the isotope effects minus one on V/K and V, respectively.

The H_2O and D_2O initial velocity data obtained for PPD-CoA were combined and globally fit to the following equation using GraFit

$$v = VAB/\{(1 + f_i IE_{V/K1})[K_{ia}K_b] + (1 + f_i IE_{V/K2})[K_aB] + (1 + f_i IE_{V/K3})[K_bA] + (1 + f_i IE_V)[AB]\} \quad (4)$$

where f_i is the fraction of isotope (^{2}H) in the reaction (0−1.0), $IE_{V/K1}$, $IE_{V/K2}$, $IE_{V/K3}$, and IE_V are the isotope effects minus one on $V/K_{ia}K_b$, V/K_a, V/K_b, and V, respectively.

Primary Kinetic Isotope Effects on Hydride Transfer. Primary kinetic isotope effects on V (^DV) and V/K ($^DV/K$) were determined for both HD-CoA and PPD-CoA at pH 7.5. Initial velocity patterns for HD-CoA were obtained using variable concentrations of NADPH or [4*S*-^{2}H]NADPH (10−100 μM) and dienoyl-CoA (1−30 μM). The kinetic parameters for PPD-CoA were obtained in a similar manner using variable concentrations of NADPH or [4*S*-^{2}H]NADPH (1−90 μM) and dienoyl-CoA (0.3−12 μM). For each dienoyl-CoA substrate, the NADPH and [4*S*-^{2}H]NADPH initial velocity data were combined and globally fit to eqs 3 and 4 using an $f_i = 0.95$ for the [4*S*-^{2}H]NADPH data.

Transient Kinetics of Substrate Binding. Transient kinetic studies of substrate binding were performed using an Applied Photophysics SX18 stopped-flow spectrophotometer in the fluorescence mode. All experiments were conducted in 100 mM KP_i containing 100 μM EDTA (pH 7.5) where the temperature was maintained at 25 ± 0.2 °C by a circulating water bath. The change in the 24DCR's intrinsic tryptophan fluorescence was monitored as a function of time for the binding of dienoyl-CoAs to the enzyme. The excitation monochromator was set to 280 nm, and a 305 nm "cut-on" filter (transparent to light with a wavelength greater than 305 nm) was used for the emitted light. In a typical experiment, a solution containing 24DCR (0.2−0.4 μM final concentration) was loaded into one syringe and mixed with a solution containing the dienoyl-CoA (0.5−40 μM final concentrations) that had been loaded into the second syringe. Binding was observed for 200 ms, collecting 1000 data points. The resulting curves for each substrate concentration were fit to the equation

$$y = A\exp(-k_{obs}t) + C \quad (5)$$

where y is the fluorescence signal, A is the observed amplitude, k_{obs} is the observed rate constant, t is the time after mixing, and C is the final fluorescence at $t = 200$ ms. The data collected from three to five separate mixing events were averaged for each determination of k_{obs}.

Binding of NADPH to the 24DCR was monitored by observing the change in NADPH fluorescence as a function of time. The excitation monochromator was set to 340 nm, and a 385 nm cut-on filter was used for the emitted light. The data were acquired as described above for variable NADPH concentrations (1−15 μM) and the resulting curves were fit to the equation

$$y = A(1 - \exp(-k_{obs}t)) + C \quad (6)$$

where y is the fluorescence signal, A is the observed amplitude, k_{obs} is the observed rate constant, t is the time after mixing, and C is the background fluorescence at $t = 0$ ms.

The secondary plots of k_{obs} vs substrate concentration [S] were fit to either eq 7 or eq 8

$$k_{obs} = k_{on}[S] + k_{off} \quad (7)$$

$$k_{obs} = \frac{Cap[S]}{K_d + [S]} + k_{off} \quad (8)$$

where k_{on} and k_{off} are the association and dissociation rate constants of substrate binding in eq 7, and Cap is the maximum rate of reaction, [S] is the substrate concentration, K_d is the true dissociation constant, and k_{off} is the dissociation rate constant in eq 8.

Transient Kinetics. Transient kinetic traces were acquired using an Applied Photophysics SX-18 stopped-flow apparatus in absorbance mode at 25 ± 0.2 °C. The optics were oriented such that the absorbance photomultiplier was positioned to observe the 10 mm light path of the flow cell. Reactions were carried out in 100 mM KP_i containing 100 μM EDTA (pH 7.5), and the change in absorbance at 340 nm was monitored as a function of time for the NADPH-dependent reductions of both HD-CoA and PPD-CoA. A solution of 24DCR and HD-CoA was prepared in buffer and loaded into one syringe and mixed with a buffered solution

containing NADPH in the second syringe. In the reverse experiment, a solution of 24DCR and NADPH was mixed with a HD-CoA solution. After mixing, the final concentrations of 24DCR, HD-CoA, and NADPH were 3, 50, and 50 μM, respectively, for both experiments. For each acquisition, 1000 data points were recorded using a logarithmic time base 10 s in duration. Data from at least three mixing events were acquired and averaged for each set of enzyme−substrate combinations.

The transient kinetics for PPD-CoA reduction were carried out in a similar manner with one exception, the final concentration of PPD-CoA was adjusted to 40 μM in order to keep the total A_{340} <2.0, the upper limit for this instrument.

The rate constant for hydride transfer for HD-CoA reduction was determined by fitting the first 1.5 s of the transient time trace to the equation

$$y = A_1(1 - \exp(-k_1 t)) + A_2 \exp(-k_2 t) - v_{ss} t + C \quad (9)$$

where y is the absorbance at 340 nm, A_1 and A_2 are the observed amplitudes, k_1 is the rate constant for the mixing event artifact, k_2 is the rate constant for hydride transfer, t is time, v_{ss} is the steady-state velocity, and C is the background absorbance.

Transient Kinetics for the Generation of Transient Spectra. Transient kinetic spectra of HD-CoA reduction were generated by acquiring data using an Applied Photophysics SX-18 stopped-flow apparatus in absorbance mode, using the 10 mm light path, at 25 ± 0.2 °C. Prior to conducting the transient kinetics, the system was flushed with reaction buffer, and the photomultiplier voltage necessary to maintain a zero absorbance at each wavelength was determined. A solution of 24DCR and HD-CoA was prepared in D_2O buffer (100 mM KP_i, 100 μM EDTA, pD 7.5) and loaded into one syringe and mixed with a D_2O buffered solution containing NADPH in the second syringe. After mixing, the concentrations of enzyme, HD-CoA, and NADPH were 5, 50, and 50 μM, respectively. For each mixing event 1000 data points were recorded using a logarithmic time base 10 s in duration. The transient time traces were collected every 2−3 nm between 245 and 365 nm, making sure to adjust the photomultiplier voltage for each successive wavelength. Three transient time traces were collected, in three successive mixing events, for each wavelength and averaged. The averaged transient time traces for 48 individual wavelengths were combined and transposed into the corresponding transient spectra, over the range of 245−365 nm, using Origin v5.0 (MicroCal). The action spectra from the burst and steady-state regions were generated by subtracting a spectrum from a time point (t_1) early in the burst from the spectrum at a time point (t_2) that occurs near the end of the burst. The action spectrum for the steady-state region was generated in a similar manner by subtracting a spectrum at an early steady-state time point (t_3) from a spectrum at a later steady-state time point (t_4). The method for generating the burst and steady-state action spectra is illustrated in Figure 1. Alternatively, the UV spectrum of the intermediate formed during the burst prior to protonation was also generated by performing the single value decomposition (SVD) analysis of the multiple wavelength transient kinetic data set using Pro-Kineticist software (Applied Photophysics).

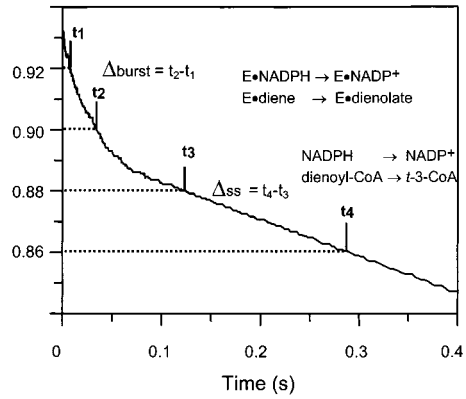

FIGURE 1: Schematic representation of the determination of the spectrum of the dienolate intermediate.

Table 1: Kinetic Parameters of 2,4-Dienoyl-CoA Reductase

substrate	k_{cat} (s^{-1})	K_m (μM)	k_{cat}/K_m (M^{-1} s^{-1}) × 10^{-6}
HD-CoA	2.1 ± 0.1	0.74 ± 0.21	2.6 ± 0.7
NADPH		4.3 ± 1.3	0.46 ± 0.13
PPD-CoA	1.8 ± 0.2	1.4 ± 0.2	1.3 ± 0.1
NADPH		21 ± 2.8	0.087 ± 0.01

24DCR-Catalyzed Exchange of the Cα Protons of trans-3-Decenoyl-CoA. The 24DCR-catalyzed exchange of the Cα protons of *trans*-3-decenoyl-CoA was monitored by ^{1}H NMR. All ^{1}H NMR spectra were acquired on a Varian Innova 600 MHz spectrometer operating at 599.908 MHz equipped with a triple resonance probe at a 6000 Hz sweep width. The ^{1}H data were acquired at 25 °C with a solvent (H_2O) presaturation pulse 1.5 s in duration. A 90° pulse with a 7.9 μs pulse width followed by a 1.7 s acquisition time was used. *trans*-3-Decenoyl-CoA (~400 μM) and $NADP^+$ (400 μM) were solubilized in phosphate-buffered D_2O (50 mM, pD 7.5), and a preliminary ^{1}H NMR spectrum was acquired. Next, 24DCR (final concentration 1 μM) was added to the NMR tube containing the *trans*-3-decenoyl-CoA and $NADP^+$, and a ^{1}H NMR spectrum was immediately acquired (t = 0 h). Subsequent spectra were then acquired every hour for a total of 10 h, where 128 transients were accumulated at each time point. An identical control experiment was conducted in the absence of 24DCR. ^{1}H NMR spectra of the control experiment were acquired at selected time intervals over an extended range, 48 h. Chemical shifts were referenced internally by use of the triplet at 2.43 ppm (t, 2H) from the 6″ methylene protons of the pantetheine backbone of CoA. ^{1}H NMR: δ 8.58 (s, 1H), 8.28 (s, 1H), 6.19 (d, 1H), 5.68 (dt, 1H, J_{trans} = 15.2 Hz, Cγ), 5.47 (dt, 1H, J_{trans} = 15.1 Hz, Cβ), 4.59 (m, 1H), 4.25 (m, 1H), 4.03 (s, 1H), 3.85 (q, 1H), 3.57 (q, 1H), 3.46 (t, 2H), 3.34 (t, 2H), 3.27 (d, 2H, Cα), 3.04 (t, 2H), 2.43 (t, 2H), 1.99 (m, 2H, Cδ), 1.32 (m, 2H, Cε), 1.24 (m, 6H), 0.89 (s, 3H), 0.84 (t, 3H), 0.76 (s, 3H).

RESULTS

Determination of Steady-State Kinetic Parameters. Initial velocity patterns were obtained using variable concentrations of dienoyl-CoA at several fixed concentrations of NADPH, and the determined kinetic parameters are given in Table 1. Double reciprocal plots gave converging lines that intersected at the left of the ordinate, suggesting a sequential kinetic mechanism (Figures 2 and 3). The K_m values of the

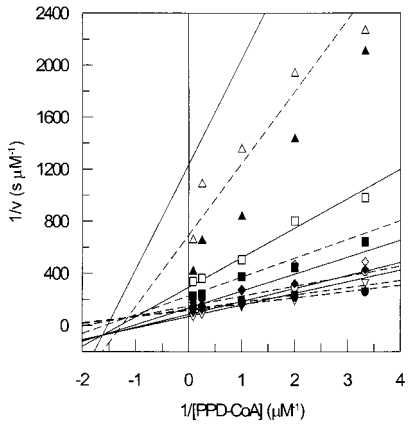

FIGURE 2: Initial velocity patterns of the 24DCR-catalyzed reduction of PPD-CoA in H_2O (open symbols) and D_2O (solid symbols). The PPD-CoA concentrations varied from 0.3 to 12 μM, and the fixed NADPH concentrations were 1 (△, ▲), 5 (□, ■), 15 (◇, ◆), 40 (○, ●), and 90 μM (▽, ▼). The slight systematic error at low NADPH concentrations arises from fitting the kinetic data globally rather than each "line" individually. The double reciprocal plot amplifies the apparent error at low velocities.

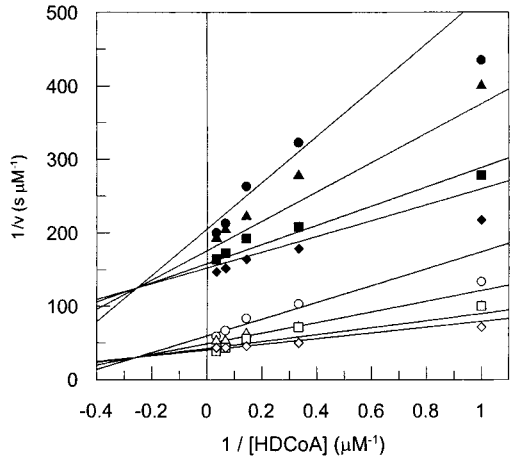

FIGURE 3: Initial velocity patterns of the 24DCR-catalyzed reduction of HD-CoA in H_2O (open symbols) and D_2O (solid symbols). The HD-CoA concentrations varied from 1 to 30 μM, and the fixed NADPH concentrations were 10 (○, ●), 20 (△, ▲), 50 (□, ■), and 100 μM (◇, ◆). The slight systematic error at low NADPH concentrations arises from fitting the kinetic data globally rather than each "line" individually. The double reciprocal plot amplifies the apparent error at low velocities.

recombinant 24DCR for NADPH and HD-CoA were 4.2 ± 1.3 μM and 0.74 ± 0.21 μM, respectively, at pH 7.5. Close examination of the data indicates that the K_m value for each substrate is less than the corresponding lowest concentration used in the initial velocity pattern. As a result, the standard error for each measurement is relatively large (>25%).

The K_m values of the recombinant 24DCR for NADPH and PPD-CoA were 21 ± 2.8 μM and 1.4 ± 0.2 μM, respectively, at pH 7.5. The lower standard errors (≈10%) result because the concentrations of both substrates in the initial velocity pattern were above and below their respective K_m values. The K_m for PPD-CoA is 7-fold less than the apparent K_m value of 9.5 μM previously reported for this substrate (*31*). One reason that our K_m value is lower is that NADPH at higher concentrations is a competitive substrate inhibitor of the CoA (*20*), which results in an increase in the apparent K_m of the CoA substrate at high NADPH.

Table 2: Primary Kinetic Isotope Effects of the 24DCR-Catalyzed Reduction of Dienoyl-CoAs

dienoyl-CoA	[4*S*-^{2}H]NADPH in H_2O	NADPH in D_2O
HD-CoA	$^{D}V/K = 1.12 \pm 0.18$	$^{D_2O}V/K = 2.85 \pm 0.95$
	$^{D}V = 1.14 \pm 0.06$	$^{D_2O}V = 3.99 \pm 0.45$
PPD-CoA	$^{D}V/K_{CoA} = 2.38 \pm 0.59$	$^{D_2O}V/K_{CoA} = 0.53 \pm 0.12$
	$^{D}V/K_{NADPH} = 2.13 \pm 0.47$	$^{D_2O}V/K_{NADPH} = 0.48 \pm 0.12$
	$^{D}V = 1.18 \pm 0.21$	$^{D_2O}V = 2.00 \pm 0.16$

When *trans*-2,*trans*-4-decadienoyl-CoA was used, substantial substrate inhibition over the concentration range 0.75−30 μM was observed (data not shown), which is in agreement with a report for the bovine enzyme (*20*). Kinetic parameters for this substrate could not be obtained because the limit of sensitivity using UV spectroscopy for these assays had been reached.

Solvent Kinetic Isotope Effects. Solvent kinetic isotope effects were measured by determining the initial velocities for HD-CoA and PPD-CoA reduction in both H_2O and D_2O (95%). Global analysis of the combined H_2O and D_2O data for each dienoyl-CoA enabled the determination of the isotope effects on V (^{D_2O}V) and V/K ($^{D_2O}V/K$) and are listed in Table 2.

The inability to accurately determine the K_m values for NADPH and HD-CoA was manifested in the solvent isotope effects, where only a single $^{D_2O}V/K$ could be determined for this combination of substrates. A large solvent isotope effect of 2.85 ± 0.85 was observed on V (^{D_2O}V), while a larger normal effect was observed on V/K ($^{D_2O}V/K = 3.99 \pm 0.45$).

In contrast, inverse kinetic isotope effects of 0.53 ± 0.12 and 0.48 ± 0.12 on V/K_{CoA} ($^{D_2O}V/K_{CoA}$) and V/K_{NADPH} ($^{D_2O}V/K_{NADPH}$), respectively, were observed with PPD-CoA. A normal ^{D_2O}V effect of 2.00 ± 0.16 was determined for this dienoyl-CoA. The normal ^{D_2O}V effect and inverse $^{D_2O}V/K$ effect for PPD-CoA indicate that different steps are rate determining for this substrate in the presence of saturating and subsaturating substrate concentrations.

Primary Deuterium Isotope Effects on Hydride Transfer. The primary deuterium kinetic isotope effects resulting from the use of [4*S*-^{2}H]NADPH are reported in Table 2. Values of $^{D}V/K$ and ^{D}V near unity were observed for the 24DCR-catalyzed reduction of HD-CoA. To verify that the *pro-4S* deuteride was transferred during the 24DCR-catalyzed reduction of HD-CoA with [4*S*-^{2}H]NADPH, the *trans*-3-hexenoyl-CoA product was isolated and analyzed by ^{1}H NMR. The NMR spectrum clearly displayed a doublet of doublets splitting pattern for the Cγ proton (*11*), indicating the presence of a single deuterium atom, originating from the [4*S*-^{2}H]NADPH, was incorporated into the Cδ position (data not shown).

Normal isotope effects on V/K_{CoA} ($^{D}V/K_{CoA}$) and V/K_{NADPH} ($^{D}V/K_{NADPH}$) of 2.38 ± 0.59 and 2.13 ± 0.47, respectively, were determined for the 24DCR-catalyzed reduction of PPD-CoA in the presence of [4*S*-^{2}H]NADPH. The similarity between these $^{D}V/K$ values is consistent with the proposed random order of nucleotide and dienoyl-CoA addition (*36*). A small normal isotope effect on V (^{D}V) of 1.18 ± 0.21 was determined for this dienoyl-CoA.

Transient Kinetics of Substrate Binding. The rate constants for association (k_{on}) and dissociation (k_{off}) of substrates and 24DCR to form both binary complexes were determined using stopped-flow fluorescence spectroscopy. A typical

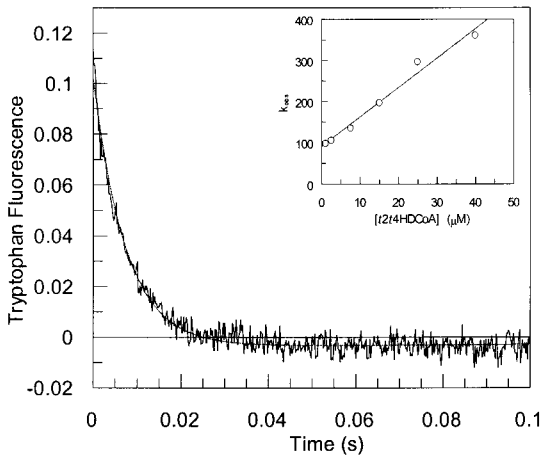

FIGURE 4: Transient kinetics of HD-CoA (7.5 μM) binding to the 24DCR (0.4 μM). The curve was fit to eq 5, and the secondary plot of k_{obs} vs HD-CoA concentration resulted in a line with a slope $= k_{on}$ and an intercept $= k_{off}$ (inset).

Table 3: Rate Constants for Substrate Binding to 24DCR

substrate	k_{on} (M^{-1} s^{-1}) $\times$ 10^{-6}	k_{off} (s^{-1})	K_d (μM)
HD-CoA	7.1 $\pm$ 0.5	90.1 $\pm$ 9.2	12.7
trans-2,*trans*-4-deca-dienoyl-CoA	10.1 $\pm$ 0.6	13.8 $\pm$ 1.3	1.4
PPD-CoA	16.8	35.5 $\pm$ 4.4	17.5 $\pm$ 2.3
NADPH	27.1 $\pm$ 3.4	94.5 $\pm$ 12.6	3.5

binding experiment is illustrated in Figure 4. The secondary plots of k_{obs} vs [S] for HD-CoA, DD-CoA, and NADPH were fit to eq 7 to obtain the values for k_{on} and k_{off} (Table 3). The dissociation constants (K_d) for the interactions of HD-CoA, DD-CoA, and NADPH with the 24DCR were calculated to be 12.7, 1.4, and 3.5 μM, respectively. The secondary plot of k_{obs} vs PPD-CoA concentration was hyperbolic, and the data were fit to eq 8, as described by Johnson (*37*), and a dissociation constant (K_d) of 17.5 $\pm$ 2.3 μM was determined.

Transient Kinetics. The transient kinetic time traces for mixing the 24DCR·HD-CoA complex with NADPH and the 24DCR·NADPH complex with HD-CoA are illustrated in Figure 5. A mixing artifact is observed in the first 10 ms for both combinations. This artifact is solely associated with the mixing of NADPH in the instrument, and a rate constant for this event was determined by fitting the transient kinetic data obtained from mixing a buffered NADPH solution (50 μM final concentration) with buffer alone and observing the change in absorbance at 340 nm as a function of time. The resulting curve was fit to eq 6, and a $k_{obs} = 196$ s^{-1} was obtained. This value is k_1 in eq 9 and was held constant in the determination of the rate constant of hydride transfer (k_2).

There is no significant difference between the E·HD-CoA vs NADPH and E·NADPH vs HD-CoA transient traces. Both time traces were fit to eq 9, where k_1 was held constant and a value of 34.2 $\pm$ 0.9 s^{-1} for k_2 was determined, which is the rate constant of hydride transfer for this substrate pair.

The transient time trace for the reduction of PPD-CoA is shown in Figure 6. For this substrate there is no observable burst as seen for HD-CoA, suggesting that a different step is rate limiting for this substrate.

Generation of the Transient Spectra for HD-CoA Reduction. The transient spectra for the 24DCR-catalyzed reduction of HD-CoA are shown in Figure 7. At $t = 0$, the absorbance

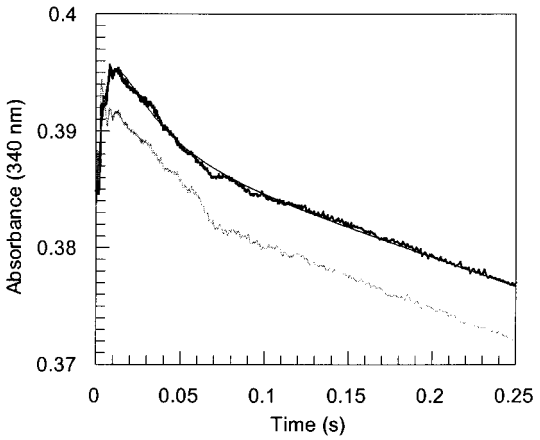

FIGURE 5: Transient kinetics of the 24DCR-catalyzed reduction of HD-CoA. The mixing of E·HD-CoA with NADPH (upper bold curve) is essentially identical to the mixing of E·NADPH with HD-CoA (lower gray curve). After mixing, the final concentrations of 24DCR, HD-CoA, and NADPH were 3, 50, and 50 μM, respectively. The absence of a lag in either curve supports the random order of substrate addition. The presence of a burst from 10 to 70 ms suggests that hydride transfer is the fast step for this substrate. Fitting the E·HD-CoA vs NADPH data to eq 9 results in a rate constant for hydride transfer of 34.2 $\pm$ 0.9 s^{-1}.

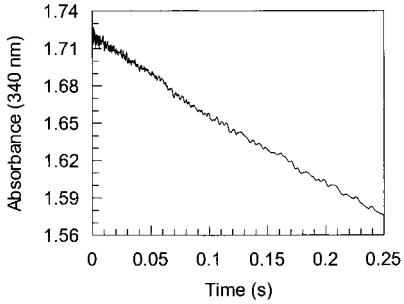

FIGURE 6: Transient kinetics of the 24DCR-catalyzed reduction of PPD-CoA. After mixing, the concentrations of 24DCR, NADPH, and PPD-CoA were 3, 50, and 40 μM, respectively. The absence of a burst indicates that a different step has become rate limiting for this substrate.

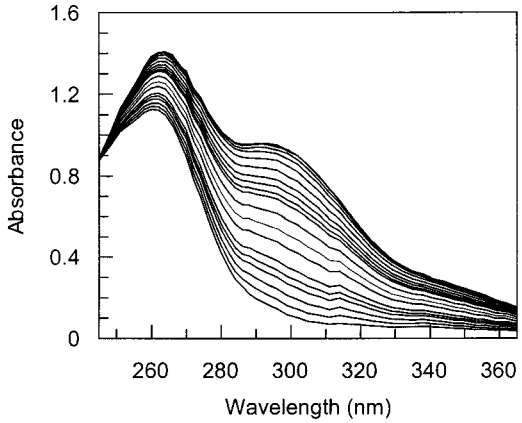

FIGURE 7: Transient spectra of the 24DCR-catalyzed reduction of HD-CoA from 0 to 10 s. The absorbance at all wavelengths decreased with time.

of HD-CoA at 296 nm and NADPH at 340 nm is clearly seen, but at $t = 10$ s the reaction is essentially complete, as evidenced by the loss of absorbance at both wavelengths. Acquiring the transient kinetic data using a logarithmic time base allowed for the generation of greater than 700 transient spectra in the first second of data acquisition with a total of

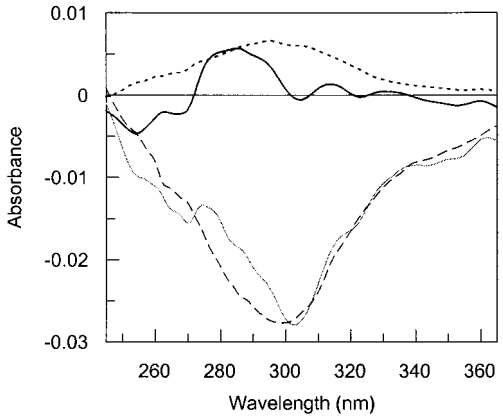

FIGURE 8: Action spectra from the burst and steady state for the 24DCR-catalyzed reduction of HD-CoA. The difference in λ_{max} between the burst action spectrum (solid gray line) and the steady-state action spectrum (dashed line) occurs presumably from the presence of an intermediate that absorbs in the burst but not in the steady state. Subtracting the steady-state action spectrum from the burst action spectrum results in the spectrum of the dienolate intermediate (bold line) that has an absorbance maximum at 286 nm. The spectrum of the intermediate generated by single value decomposition has a maximum at 294 nm (bold dotted line).

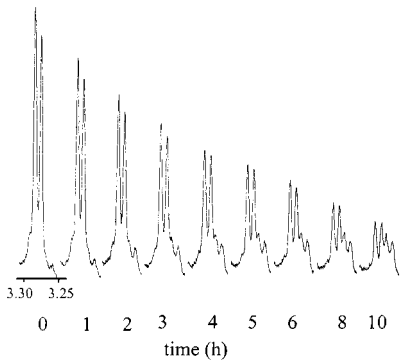

FIGURE 9: ^{1}H NMR spectra of *trans*-3-decenoyl-CoA over the region 3.31−3.24 ppm. The sample contained 50 mM KP_i, 400 μM $NADP^+$, and 1 μM 24DCR in D_2O at pD 7.5. In the presence of 24DCR, the Cα proton resonance at 3.27 ppm decreases as a function of time, indicating that the 24DCR facilitates the exchange of the Cα protons with solvent-derived deuterium. The appearance of a doublet at 3.25 ppm results from the isotope effect on the chemical shift of the Cα proton of [2-^{2}H]-*trans*-3-decenoyl-CoA.

1000 transient spectra over the 10 s time course. The method for generating the spectrum of the dienolate intermediate that forms in the burst prior to proton transfer is illustrated in Figure 1. The resulting action spectra from the burst and steady-state regions of the transient time trace are shown in Figure 8. The spectrum of the dienolate intermediate, generated by subtracting the steady-state action spectrum from the burst action spectrum, is shown in Figure 8. The dienolate intermediate has a λ_{max} of 286 nm. This is in agreement with the spectrum of the intermediate obtained by performing the single value decomposition of the transient spectra data set using Pro-Kineticist. The spectrum of the intermediate generated by the SVD has a λ_{max} of 294 nm (Figure 8).

Exchange of the Cα Protons in trans-3-Decenoyl-CoA. The ^{1}H NMR spectrum over the region 3.31−3.24 ppm is shown in Figure 9. Following the addition of 24DCR the resonance at 3.27 ppm, corresponding to the Cα protons of *trans*-3-decenoyl-CoA, decreases substantially over 10 h due to the incorporation of a solvent-derived deuterium. The decrease in intensity in the Cα resonance is accompanied by the appearance of a doublet at 3.25 ppm, which is attributed to the isotope effect on δ_H resulting from the replacement of one of the Cα protons with deuterium. Integration of the region 3.30−3.24 ppm, for the $t = 10$ h spectrum, gave a value of 0.27 when normalized to the internal integration standard at 2.43 ppm, given a set value of 2.00 protons. The incorporation of ^{2}H into the Cα position was confirmed by the change in the splitting pattern for the Cβ proton resonance, at 5.47 ppm, from a doublet of triplets to a doublet of doublets (data not shown) (*11*). Incorporation of ^{2}H into the Cα position of *trans*-3-decenoyl-CoA was also observed in the absence of 24DCR. After 48 h, the intensity of the Cα proton resonance had decreased but to a lesser extent, normalized integration of 0.60, when compared to the enzyme-catalyzed exchange. This indicates that the enzyme-catalyzed exchange occurs at least five times faster than the non-enzyme-catalyzed exchange.

DISCUSSION

The Kinetic Mechanism of Dienoyl-CoA Reduction. The double reciprocal plots for both HD-CoA and PPD-CoA reduction (Figures 2 and 3) display a series of nonparallel intersecting lines, indicating that the 24DCR proceeds via a sequential mechanism. The normal isotope effects on V/K_{CoA} ($^DV/K_{CoA} = 2.38 \pm 0.59$) and V/K_{NADPH} ($^DV/K_{NADPH} = 2.13 \pm 0.47$) for PPD-CoA reduction are essentially the same (within experimental error), suggesting a random order of nucleotide and substrate addition. The random mechanism was further supported by transient kinetics. The transient kinetics of substrate binding demonstrated that DD-CoA, HD-CoA, and PPD-CoA could bind to the 24DCR in the absence of the reduced pyridine nucleotide cofactor. Similarly, NADPH was shown to bind to the enzyme [$k_{on} = (27.1 \pm 3.4) \times 10^{-6}$ M^{-1} s^{-1}] in the absence of a dienoyl-CoA, further supporting a random mechanism. In addition, the transient kinetics of HD-CoA reduction (Figure 5) support a random mechanism. The transient kinetic trace for mixing an E·HD-CoA complex with NADPH was the same as the transient time trace that resulted from mixing an E·NADPH complex with HD-CoA. The absence of a lag in either curve provides additional evidence for the random order of substrate addition.

The Chemical Mechanism of Dienoyl-CoA Reduction. In the 24DCR-catalyzed reduction of dienoyl-CoAs, a hydride equivalent from NADPH must be transferred to the dienoyl-CoA as well as the incorporation of a solvent-derived proton to yield the resulting *trans*-3-enoyl-CoA product. These chemical steps may occur either simultaneously, as in a concerted mechanism, or successively, as in a stepwise mechanism. The experimental results presented in this report demonstrate that the 24DCR-catalyzed reaction proceeds through a stepwise mechanism. The kinetic isotope effect and solvent isotope effects studies support the stepwise mechanism. Small normal kinetic isotope effects on V/K ($^DV/K = 1.12 \pm 0.18$) and V ($^DV = 1.14 \pm 0.06$) were observed for the reduction of HD-CoA, but large solvent isotope effects on V ($^{D_2O}V = 2.85 \pm 0.95$) and V/K ($^{D_2O}V/K = 3.99 \pm 0.45$) were observed. These isotope effects indicate that a protonation step is rate limiting for the reduction of HD-CoA. This is an interesting finding because the isoto-

Scheme 1

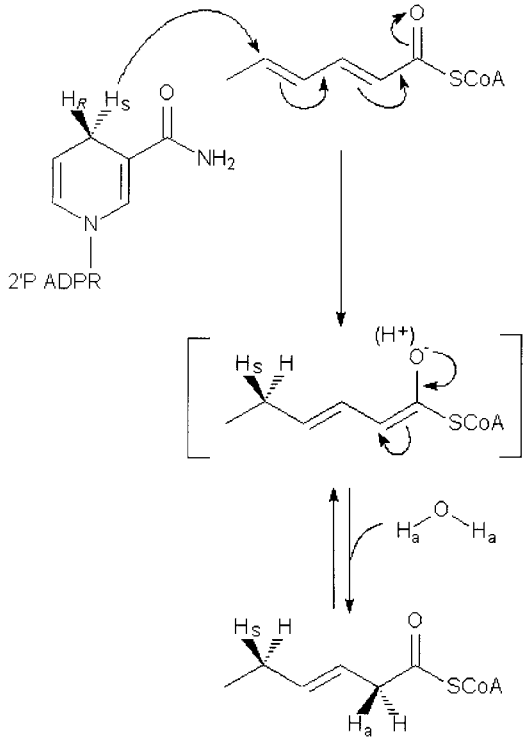

pically sensitive steps have been reversed when compared to studies of the homologous InhA enoyl-thiolester reductase from *M. tuberculosis* (*5*, *26*). The diene moiety in PPD-CoA gains additional stability as a result of conjugation with the phenyl ring. As a result, the isotopically sensitive step is reversed where normal kinetic isotope effects on both V/K_{CoA} ($^{D}V/K_{CoA} = 2.38 \pm 0.59$) and V/K_{NADPH} ($^{D}V/K_{NADPH} = 2.13 \pm 0.47$) were observed. The inverse solvent isotope effects on V/K_{CoA} ($^{D_2O}V/K_{CoA} = 0.53 \pm 0.12$) and V/K_{NADPH} ($^{D_2O}V/K_{NADPH} = 0.48 \pm 0.12$) may potentially result from the desolvation of this hydrophobic substrate. Therefore, a stepwise mechanism is supported because hydride transfer or protonation can be rate limiting depending on the dienoyl-CoA substrate.

For PPD-CoA, a small normal isotope effect on V ($^{D}V = 1.18 \pm 0.21$) and a larger solvent isotope effect on V ($^{D_2O}V = 2.00 \pm 0.16$) were determined. These isotope effects are opposite of the isotope effect observed on both V/K_{CoA} and V/K_{NADPH} ($^{D}V/K$ and $^{D_2O}V/K$), which suggests that there is an isotopically sensitive step that occurs after substrate binding but prior to the first chemical step.

The transient kinetics of both HD-CoA and PPD-CoA reduction confirm the conclusions from the isotope effect studies. For HD-CoA reduction, the rate-determining step was protonation, and as predicted a burst was observed in the transient kinetics corresponding to the rapid transfer of a hydride equivalent (Figure 5). Conversely, no burst was observed in the transient kinetics of PPD-CoA reduction (Figure 6), demonstrating that hydride transfer is rate limiting, which agrees with the kinetic isotope effects on V/K. The stepwise mechanism is illustrated in Scheme 1, where hydride transfer occurs forming a dienolate intermediate which is subsequently protonated to yield the *trans*-3-enoyl-CoA.

Previous studies on the Δ^5-3-ketosteroid isomerase indicate that the chemical mechanism of this enzyme proceeds

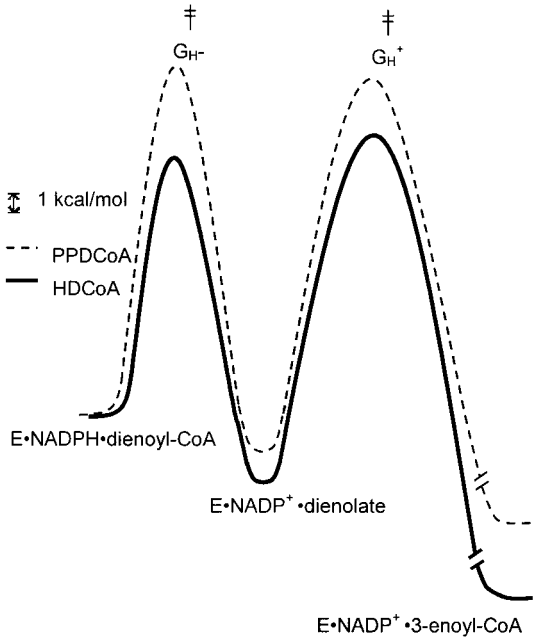

FIGURE 10: Reaction coordinate diagrams for the reduction of HD-CoA (solid line) and PPD-CoA (dashed line). The enzyme−substrate ternary complexes were arbitrarily set to the same energy level while the heights of the barriers were defined by k_{cat}. The relative heights of the hydride transfer and proton transfer transition states were established by the $^{D}V/K$ values for each substrate, and the energy level of the intermediate was defined by the transient kinetics. The absolute energy of the PPD-CoA dienolate intermediate must be greater than the HD-CoA dienolate intermediate but is undefined.

through a dienolate intermediate (*38*, *39*). Pollack et al. have directly observed the base-catalyzed formation of the dienolate intermediate of 5-androstene-3,17-dione which has an absorbance maximum at 256 (*40*). The absorbance maximum of the dienolate intermediate formed during HD-CoA reduction (Figure 8) is red shifted 30 nm to 286 nm. Presumably, this red shift results from directly bonding the dienolate to the sulfur of CoA. The SVD analysis of the multiwavelength transient kinetic data results in an intermediate spectrum with a λ_{max} that is red shifted even further to 294 nm. The direct observation of the dienolate intermediate (Figure 8) provides strong evidence for a stepwise mechanism.

These results are schematically represented in the reaction coordinate diagrams for both HD-CoA and PPD-CoA in Figure 10. The relative heights of the hydride transfer and proton transfer transition states were established by the $^{D}V/K$ values for each substrate. These reaction coordinate diagrams illustrate that because the free energy of the transition states for both elementary steps are similar, the modest changes in energetics introduced by the extra conjugation PPD-CoA can alter the rate-determining transition state. The energy of the HD-CoA-derived dienolate intermediate was established by k_{cat} for this substrate, which was largely controlled by the proton transfer step as evidenced by the ^{D_2O}V, the transient burst in NADPH oxidation, and the observation of the dienolate intermediate. If the extinction coefficient for the dienolate were known, this value could be set precisely. Our attempts to synthesize a model *N*-acetylcysteamine thiolester dienolate to determine this extinction coefficient by basic titration of *N*-acetyl-*S*-*trans*-3-hexenoylcysteamine in aprotic solvents were unsuccessful. The energy of the dienolate obtained following hydride transfer to PPD-CoA must be

Scheme 2

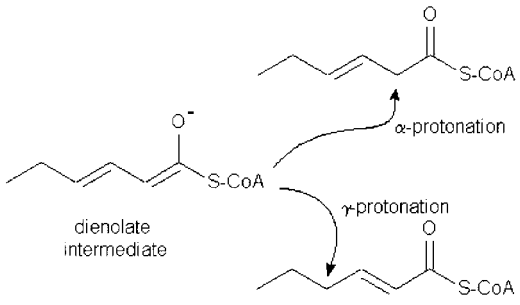

high enough so that there is minimal accumulation at the steady state. The large free energy decrease in the overall reaction has to occur following protonation of the intermediate rather than just after hydride transfer, or else the $^{D_2O}V/K$ isotope effects with HD-CoA as the substrates would be unity; i.e., formation of the dienolate intermediate must be reversible. This is consistent with the very small enhancement of the of solvent isotope exchange into the α-carbon catalyzed by 24DCR. Other enzymes that have stabilized a thiolester enol(ate) readily catalyzed the solvent exchange of the α-proton (*41*−*47*).

This suggestion that the dienolate is not unusually stabilized during this reaction is corroborated by several other observations. A substantial red shift of the dienoyl-CoA expected from polarization of the enoyl-CoA substrates in the binary or ternary complexes has not been detected (data not shown). In two other classes of enzymes that utilize enoyl-thiolesters as substrates, the acyl-CoA dehydrogenases, e.g., medium chain acyl-CoA dehydrogenase, and the enoyl-CoA isomerase/hydratase family of enzymes, a strong polarization of the carbonyl group that stabilizes an enol(ate) intermediate has been observed by UV and Raman spectroscopy (*48*−*50*). In these enzymes the thiolester carbonyl is positioned to form two H-bonds (*51*, *52*). Surprisingly, in the (di)enoyl-CoA reductases, there appears to be no requirement for a strong H-bond to the thiolester substrate or to an enolate intermediate. In the crystal structure of the ternary InhA·NAD^+·*N*-acetyl-*S*-hexadecenoylcysteamine complex [1BVR in the Protein Data Bank (*53*)], there are no H-bond donors within 3.0 Å (*54*). In InhA Tyr-158 could potentially provide a H-bond, but mutational analysis indicates that both Y158F and Y158S mutants retain significant activity, indicating that this potential H-bond is not critical (*26*). In part, this absence of carbonyl polarization may be a reflection on the ease of hydride transfer relative to protonation of the enolate intermediate. With proton transfer to the enolate intermediate being the rate-determining step, further stabilization of the anionic intermediate would increase the activation energy for proton transfer and result in a decrease in k_{cat}.

This kinetic difficulty of protonating the dienolate permits a rationalization of the regiospecificity of the reaction. Protonation at the α-carbon of the dienolate generates the thermodynamically less favored unconjugated 3-enoyl-CoA as shown in Scheme 2. The formation of this thermodynamically disfavored product also requires an additional metabolic step to isomerize the 3-enoyl-CoA to the *trans*-2-enoyl-CoA so that it can be further metabolized through the β-oxidation pathway. However, protonation at the α-carbon is kinetically favored by the greater electron density at this carbon, and since protonation is the rate-determining step, the most favored kinetic pathway has been followed. In the *E. coli* 24DCR, the hydride equivalent is provided by a flavin, which results in a thermodynamically less favorable hydride transfer step, increasing the probability that hydride transfer is the rate-determining step. Notably, in this enzyme protonation occurs at the γ-carbon, and there is a significant polarization of the carbonyl (*55*).

ACKNOWLEDGMENT

We thank Dr. Dale Ray for his assistance in acquiring the arrayed ^{1}H NMR spectra and Dr. Simon Senior for many helpful discussions regarding the stopped-flow instrument.

REFERENCES

1. Kikuchi, S., and Kusaka, T. (1984) *J. Biochem. (Tokyo) 96*, 841−848.
2. Inui, H., Miyatake, K., Nakano, Y., and Kitaoka, S. (1984) *Eur. J. Biochem. 142*, 121−126.
3. Chang, S. I., and Hammes, G. G. (1989) *Proc. Natl. Acad. Sci. U.S.A. 86*, 8373−8376.
4. Bergler, H., Fuchsbichler, S., Hogenauer, G., and Turnowsky, F. (1996) *Eur. J. Biochem. 242*, 689−694.
5. Quemard, A., Sacchettini, J. C., Dessen, A., Vilcheze, C., Bittman, R., Jacobs, W. R., Jr., and Blanchard, J. S. (1995) *Biochemistry 34*, 8235−8241.
6. Banerjee, A., Dubnau, E., Quemard, A., Balasubramian, K. S., Wilson, T., Collins, D., de Lisle, G., and Jacobs, W. R. (1994) *Science 263*, 227−230.
7. Heath, R. J., Yu, Y. T., Shapiro, M. A., Olson, E., and Rock, C. O. (1998) *J. Biol. Chem. 273*, 30316−30320.
8. Parikh, S. L., Xiao, G., and Tonge, P. J. (2000) *Biochemistry 39*, 7645−7650.
9. Heath, R. J., Rubin, J. R., Holland, D. R., Zhang, E., Snow, M. E., and Rock, C. O. (1999) *J. Biol. Chem. 274*, 11110−11114.
10. Stewart, M. J., Parikh, S., Xiao, G., Tonge, P. J., and Kisker, C. (1999) *J. Mol. Biol. 290*, 859−865.
11. Fillgrove, K. F., and Anderson, V. E. (2000) *Biochemistry 39*, 7001−7011.
12. Katan, M. B., Zock, P. L., and Mensink, R. P. (1995) *Annu. Rev. Nutr. 15*, 473−493.
13. Sinclair, H. M. (1990) *Biochem. Soc. Trans. 18*, 756−761.
14. Mensink, R. P., Zock, P. L., Katan, M. B., and Hornstra, G. (1992) *J. Lipid Res. 33*, 1493−1501.
15. Gurvitz, A., Rottensteiner, H., Kilpelainen, S. H., Hartig, A., Hiltunen, J. K., Binder, M., Dawes, I. W., and Hamilton, B. (1997) *J. Biol. Chem. 272*, 22140−22147.
16. Geisbrecht, B. V., Liang, X., Morrell, J. C., Schulz, H., and Gould, S. J. (1999) *J. Biol. Chem. 274*, 25814−25820.
17. Chen, L. S., Jin, S. J., and Tserng, K. Y. (1994) *Biochemistry 33*, 10527−10534.
18. Luthria, D. L., Baykousheva, S. P., and Sprecher, H. (1995) *J. Biol. Chem. 270*, 13771−13776.
19. Cuebas, D., and Schulz, H. (1982) *J. Biol. Chem. 257*, 14140−14144.
20. Dommes, V., and Kunau, W. H. (1984) *J. Biol. Chem. 259*, 1781−1788.
21. Kimura, C., Kondo, A., Koeda, N., Yamanaka, H., and Mizugaki, M. (1984) *J. Biochem. (Tokyo) 96*, 1463−1469.
22. Reynolds, K. A., and Holland, K. A. (1997) *Chem. Soc. Rev. 26*, 337−343.
23. Saito, K., Kawaguchi, A., Seyama, Y., Yamakawa, T., and Okuda, S. (1981) *Eur. J. Biochem. 116*, 581−586.
24. Liu, H. B., Wallace, K. K., and Reynolds, K. A. (1997) *J. Am. Chem. Soc. 119*, 2973−2979.
25. Anderson, V. E., and Hammes, G. G. (1984) *Biochemistry 23*, 2088−2094.
26. Parikh, S., Moynihan, D. P., Xiao, G., and Tonge, P. J. (1999) *Biochemistry 38*, 13623−13634.

27. Fawcett, T., Copse, C. L., Simon, J. W., and Slabas, A. R. (2000) *FEBS Lett. 484*, 65−68.
28. Bernert, J. T., Jr., and Sprecher, H. (1977) *J. Biol. Chem. 252*, 6736−6744.
29. Meloche, H. P., and Monti, C. T. (1975) *Anal. Biochem. 68*, 316−320.
30. Thomason, S. C., and Kubler, D. G. (1968) *J. Chem. Educ. 45*, 546−547.
31. Nada, M. A., Shoukry, K., and Schulz, H. (1994) *Lipids 29*, 517−521.
32. Fillgrove, K. L., Mizugaki, M., and Anderson, V. E. (1999) *Protein Expression Purif. 17*, 57−63.
33. Mostad, S. B., Helming, H. L., Groom, C., and Glasfeld, A. (1997) *Biochem. Biophys. Res. Commun. 233*, 681−686.
34. Klaidman, L. K., Leung, A. C., and Adams, J. D., Jr. (1995) *Anal. Biochem. 228*, 312−317.
35. Glasoe, P. K., and Long, F. A. (1960) *J. Phys. Chem. 64*, 188−190.
36. Cook, P. F. (1991) in *Enzyme Mechanism from Isotope Effects* (Cook, P. F., Ed.) pp 203−230, CRC Press, Boca Raton, FL.
37. Johnson, K. A. (1992) in *Enzymes (3rd Ed.)* pp 1−61, Academic Press, San Diego, CA.
38. Xue, L. A., Kuliopulos, A., Mildvan, A. S., and Talalay, P. (1991) *Biochemistry 30*, 4991−4997.
39. Kuliopulos, A., Mildvan, A. S., Shortle, D., and Talalay, P. (1989) *Biochemistry 28*, 149−159.
40. Pollack, R. M., Mack, J. P. G., and Eldin, S. (1987) *J. Am. Chem. Soc. 109*, 5048−5050.
41. Biellmann, J. F., and Hirth, C. G. (1970) *FEBS Lett. 9*, 335−336.
42. Gilbert, H. F. (1981) *Biochemistry 20*, 5643−5649.
43. Mayer, J. M., Young, M., Testa, B., and Etter, J. C. (1989) *Helv. Chim. Acta 72*, 1225−1232.
44. Miziorko, H. M., Behnke, C. E., and Ahmad, F. (1989) *Biochemistry 28*, 5759−5764.
45. Wlassics, I. D., and Anderson, V. E. (1989) *Biochemistry 28*, 1627−1633.
46. Anderson, V. E., Bahnson, B. J., Wlassics, I. D., and Walsh, C. T. (1990) *J. Biol. Chem. 265*, 6255−6261.
47. D'Ordine, R. L., Bahnson, B. J., Tonge, P. J., and Anderson, V. E. (1994) *Biochemistry 33*, 14733−14742.
48. Trievel, R. C., Wang, R., Anderson, V. E., and Thorpe, C. (1995) *Biochemistry 34*, 8597−8605.
49. Tonge, P. J., Anderson, V. E., Fausto, R., Kim, M., Pusztai-Carey, M., and Carey, P. R. (1995) *J. Biol. Spectrosc. 1*, 387−394.
50. Taylor, K. L., Xiang, H., Liu, R. Q., Yang, G., and Dunaway-Mariano, D. (1997) *Biochemistry 36*, 1349−1361.
51. Engst, S., Vock, P., Wang, M., Kim, J. J., and Ghisla, S. (1999) *Biochemistry 38*, 257−267.
52. Engel, C. K., Mathieu, M., Zeelen, J. P., Hiltunen, J. K., and Wierenga, R. K. (1996) *EMBO J. 15*, 5135−5145.
53. Berman, H. M., Westbrook, J., Feng, Z., Gilliland, G., Bhat, T. N., Weissig, H., Shindyalov, I. N., and Bourne, P. E. (2000) *Nucleic Acids Res. 28*, 235−242.
54. Rozwarski, D. A., Vilcheze, C., Sugantino, M., Bittman, R., and Sacchettini, J. C. (1999) *J. Biol. Chem. 274*, 15582−15589.
55. Liang, X., Thorpe, C., and Schulz, H. (2000) *Arch. Biochem. Biophys. 380*, 373−379.

BI0111606